Hindawi
Wireless Communications and Mobile Computing
Volume 2021, Article ID 6648887, 11 pages
https://doi.org/10.1155/2021/6648887

Research Article

A Low-Profile Circularly Polarized Conical-Beam Antenna with Wide Overlap Bandwidth

Wei He,[1] Yejun He,[1] Long Zhang,[1] Sai-Wai Wong,[1] Wenting Li,[1] and Amir Boag[2]

[1]*College of Electronics and Information Engineering, Shenzhen University, Shenzhen 518060, China*
[2]*School of Electrical Engineering, Tel Aviv University, Tel Aviv 69978, Israel*

Correspondence should be addressed to Yejun He; heyejun@126.com

Received 15 October 2020; Revised 26 January 2021; Accepted 6 February 2021; Published 28 February 2021

Academic Editor: liang wu

In this paper, a low-profile circularly polarized (CP) conical-beam antenna with a wide overlap bandwidth is presented. Such an antenna is constructed on the two sides of a square substrate. The antenna consists of a wideband monopolar patch antenna fed by a probe in the center and two sets of arc-hook-shaped branches. The monopolar patch antenna is loaded by a set of conductive shorting vias to achieve a wideband vertically polarized electric field. Two sets of arc-hook-shaped parasitic branches connected to the patch and ground plane can generate a horizontally polarized electric field. To further increase the bandwidth of the horizontally polarized electric field, two types of arc-hook-shaped branches with different sizes are used, which can generate another resonant frequency. When the parameters of the arc-hook-shaped branches are reasonably adjusted, a 90° phase difference can be generated between the vertically polarized electric field and the horizontally polarized electric field, so that the antenna can produce a wideband CP radiation pattern with a conical beam. The proposed antenna has a wide impedance bandwidth ($|S_{11}| < -10$ dB) of 35.6% (4.97-7.14 GHz) and a 3 dB axial ratio (AR) bandwidth at phi = 0° and theta = 35° of about 30.1% (4.97-6.73 GHz). Compared with the earlier reported conical-beam CP antennas, an important feature of the proposed antenna is that the AR bandwidth is completely included in the impedance bandwidth, that is, the overlap bandwidth of $|S_{11}| < -10$ dB and AR < 3 dB is 30.1%. Moreover, the stable omnidirectional conical-beam radiation patterns can be maintained within the whole operational bandwidth.

1. Introduction

Circularly polarized (CP) antennas are widely used in modern wireless communication because of their inherent characteristics, such as reduced multipath fading and elimination of the polarization mismatch between the transmitting antenna and the receiving antenna [1]. Furthermore, CP antennas with conical-beam radiation have been widely used in the satellite communication, indoor communication, and vehicular communication for their many advantages, such as omnidirectional radiation over a wider range of elevation angles [2–6]. With the proliferation of users and the lack of spectrum resources, wideband CP antennas are increasingly favored by various manufacturers [7]. In [8], the axis-symmetric TM01 and TE01 orthogonal modes in a circular aperture were simultaneously excited to produce CP conical-beam pattern. However, the axial ratio (AR) bandwidth is only 4.8%. In addition, by loading a CP circular patch antenna with a conical beam by a set of complementary V-shaped slits, the antenna is miniaturized, but its operating bandwidth is very narrow, only 3.5% [9]. In [10], arc-shaped patches and a disk-loaded feeding pin were utilized to realize omnidirectional conical-beam CP radiation, but the operating bandwidth was still very narrow. To that end, there have been many efforts and studies on wideband CP conical-beam antennas [11–21]. A wideband CP antenna consisting of a torus knot and a feeding probe with a conical-beam radiation pattern is proposed in [11]. An upper parasitic notched patch loaded on a lower notched circular patch with a capacitive feeding could achieve wideband CP conical-beam radiation with a 3 dB axial ratio (AR) bandwidth of 10% [12]; however, it is a multilayer substrate structure. A multilayer patch CP antenna with a conical beam fed by a hybrid coupler is presented in [13]. Although dual-band CP radiation is realized,

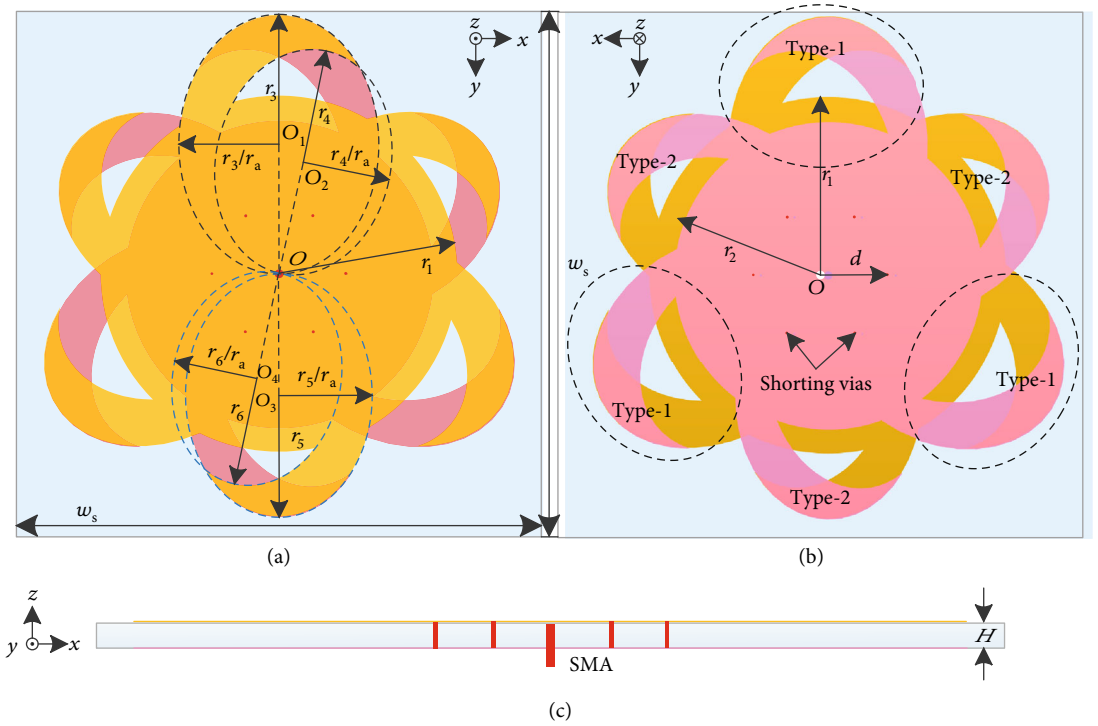

FIGURE 1: Geometry of the proposed antenna. (a) Top view. (b) Bottom view. (c) Side view.

the structure is complicated and a large reflector plane is required. In [14], a bird nest antenna with a wideband CP conical-beam radiation is proposed. A CP conical-beam antenna designed based on parasitic elements placed around the centrally fed monopole is presented in [15]. By using four microstrip line fed slot patches with truncated diagonal corners to realize CP, conical-beam radiation with the operating bandwidth of 12.2% was proposed in [16]. The antenna consists of a shorted monopolar patch proximity fed by a disk-loaded coaxial cable and two sets of curved branches sequentially located along the radiating edges as described in [17]. Although the antennas mentioned above achieve wideband CP conical-beam or omnidirectional radiation, they were all 3D structures or multilayer structures, which were not well suited for low-cost manufacturing and integration. To reduce the antenna complexity and expand the bandwidth, some low-profile patch antennas have been investigated. A low-profile patch antenna with a modified ground plane and seven curved branches is studied in [18]. Later, a circular patch antenna consisting of a wideband monopolar patch and eight parasitic loop stubs was reported in [19]. In [20], by introducing curved branches at both the patch and ground plane and making an angle between them, the antenna obtained an impedance bandwidth of 19.6% (2.16-2.63 GHz) and AR bandwidth of 27.6% (2.05-2.7 GHz). A wideband conical-beam CP antenna based on the SIW cavity was proposed in [21], which has a -10 dB impedance bandwidth of 20.4% (5.54-6.8 GHz) and AR bandwidth of 17% (5.65-6.7 GHz). In [22], the conical-beam CP antenna used five identical arc-hook branches to connect the patch and ground plane of the monopolar patch and can obtain a wide impedance bandwidth of 17.5% (5.7-6.75 GHz) and AR bandwidth of 26.5% (5.19-6.78 GHz). Although these antennas usually exhibit a low-profile structure and wide bandwidth, their operating bandwidths were still lower than 30%. Even more important disadvantage was that these antennas had relatively narrow overlap bandwidth of $|S_{11}| < -10$ dB and AR < 3 dB.

In this paper, we proposed a novel low-profile wideband conical-beam CP antenna, which has a wide impedance bandwidth, wide AR bandwidth, and wide overlap bandwidth (bandwidth of $|S_{11}| < -10$ dB and AR < 3 dB simultaneously). The proposed antenna is designed with a center fed wideband monopolar patch, six conductive shorting vias, and two sets of arc-hook-shaped branches. The wideband vertical polarization is generated by a conventional monopolar patch antenna with six conductive shorting vias. Compared with the antenna in [22], when the size of the arc-hook-shaped branches is different, a wider horizontal polarization bandwidth can be obtained. As a result, the CP conical-beam antenna with wide overlap bandwidth can be designed. The measured impedance bandwidth of $|S_{11}| < -10$ dB and AR bandwidth of AR < 3 dB of proposed antenna are 35.6% (4.97-7.14 GHz) and 30.1% (4.97-6.73 GHz), respectively. More importantly, the AR bandwidth of the proposed antenna is completely contained in the impedance bandwidth, that is, the overlap bandwidth of $|S_{11}| < -10$ dB and AR < 3 dB is 30.1%. The antenna can be used in satellite communication, indoor communication, and vehicle communication systems.

2. Antenna Design and Analysis

Figure 1 shows the geometry of the proposed wideband CP conical-beam antenna which is printed on a $w_s \times w_s$ mm^2

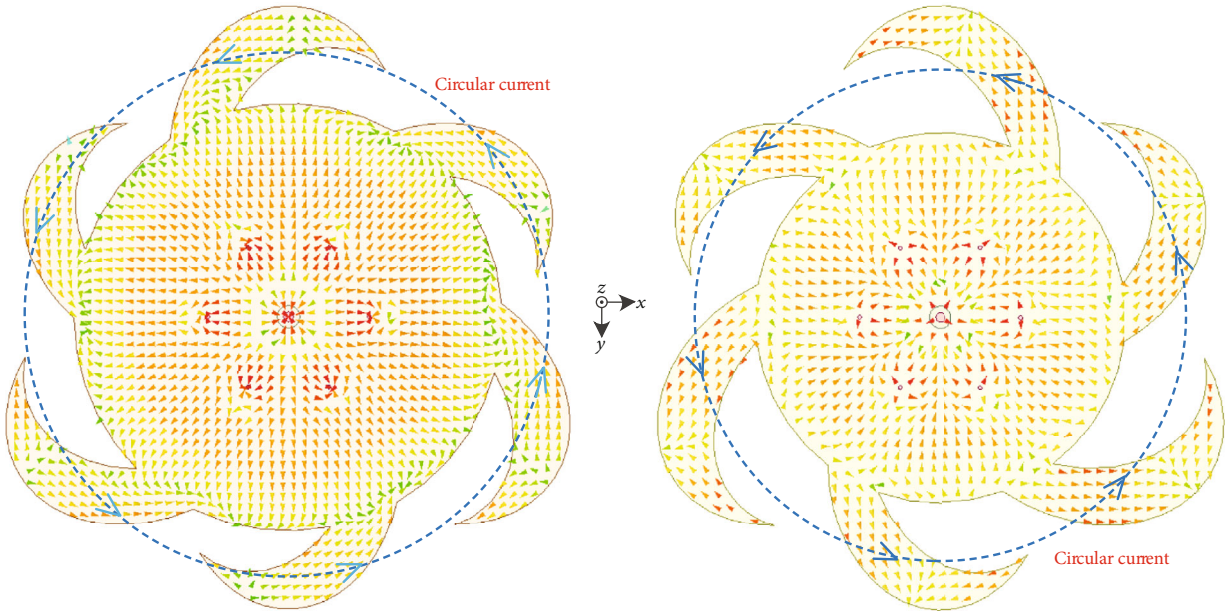

Figure 2: Current distribution at 6 GHz for the proposed antenna.

Table 1: Parameters of the proposed antenna shown in Figure 1 (r_a denotes the ratio of major axis to minor axis of ellipse).

Parameter	Value	Parameter	Value	Parameter	Value
r_1	22 mm	r_5	15 mm	d	8.3 mm
r_2	19 mm	r_6	13.3 mm	α	12 deg
r_3	16 mm	r_a	1.3	w_s	65 mm
r_4	14.1 mm	D	0.2 mm	H	3 mm

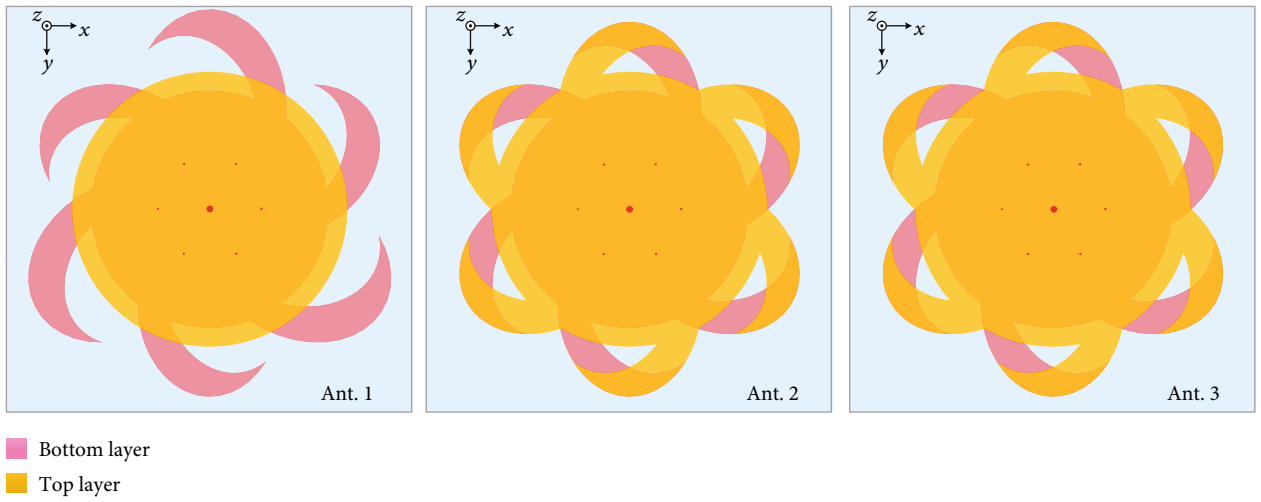

Figure 3: Antenna design evolution.

FR4 substrate. The antenna consists of two sets of arc-hook-shaped branches and a center fed monopolar patch connected to a set of shorting vias. The monopole patch antennas with two circular patches are printed on both sides of the substrate. The circular patch on the top side is slightly larger and its radius is r_1, while the circular patch on the bottom side is slightly smaller and its radius is r_2. The shorting vias are evenly arranged round the center, their diameters are denoted by D, and the distance between the center of the antenna and each shorting via is denoted by$d$. As shown in Figure 1, there are two types of arc-hook-shaped branches, denoted as Type-1 and Type-2 branches, where the size of

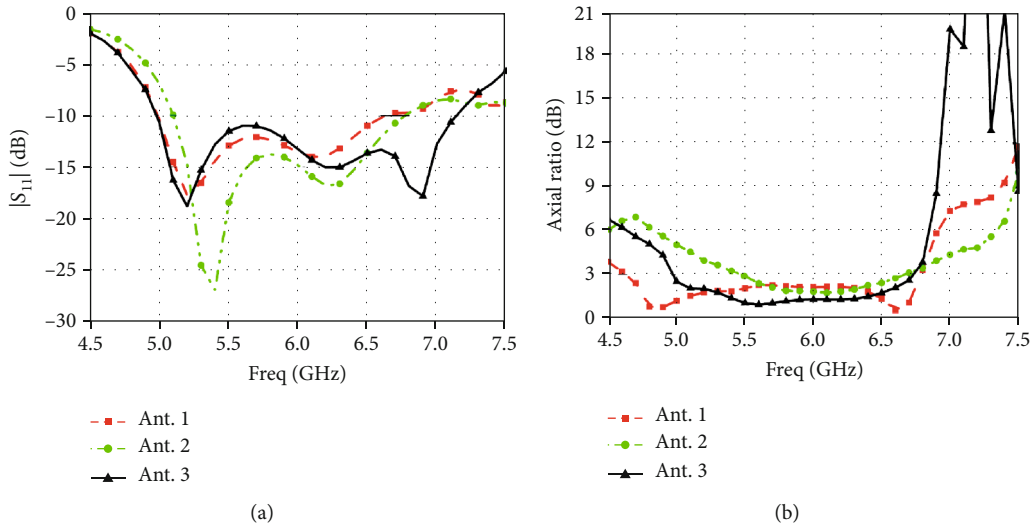

Figure 4: Simulation performance for Ant. 1-3. (a) $|S_{11}|$. (b) AR.

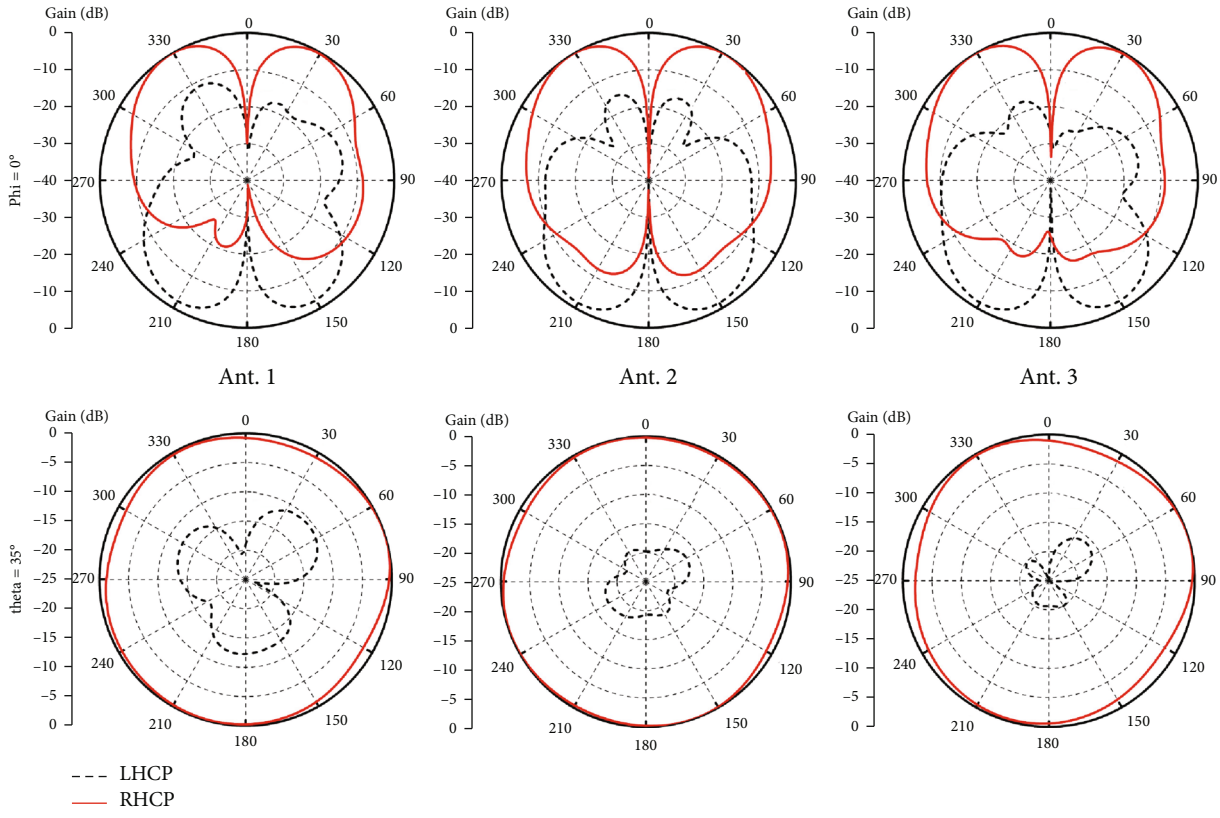

Figure 5: Simulated radiation patterns for Ant. 1-3.

Type-1 branches is slightly larger than that of Type-2 ones ($r_3 > r_5$, $r_4 > r_6$). Each arc-hook-shaped branch can be formed after a small ellipse is cut by a big ellipse as shown in Figure 1(a). Each set of arc-hook-shaped branches is composed of three Type-1 branches and three Type-2 branches. One set is arranged on the top of the substrate in a clockwise direction and connected with the upper patch of the monopolar, while the other set is a mirror image relative to the y-axis of the previous set, which is arranged on the bottom of substrate in an anticlockwise direction and connected with the ground plane. The monopolar patch and arc-hook-shaped branches can excite the vertically polarized electric field and the horizontally polarized electric field, respectively. Properly adjusting the size of the arc-hook-shaped branches

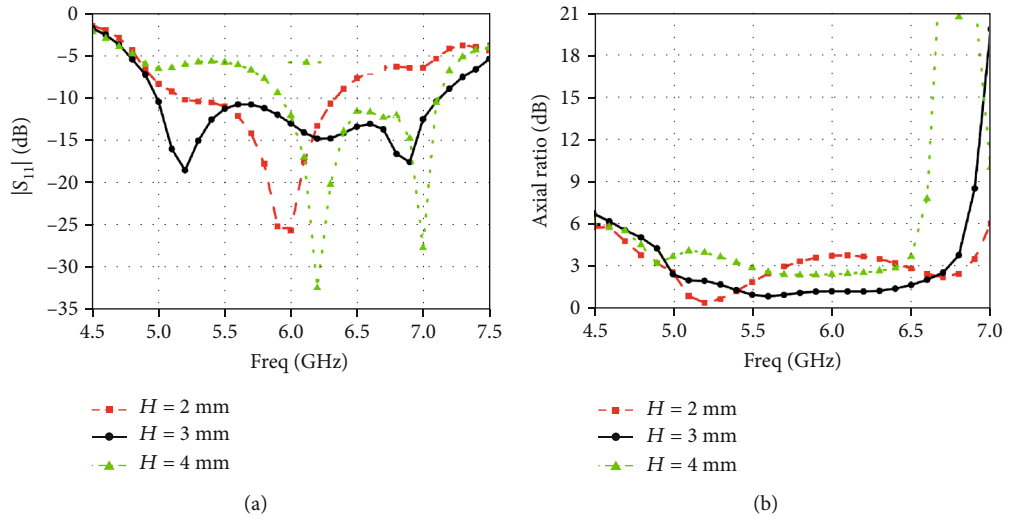

Figure 6: $|S_{11}|$ and AR with different values of H. (a) $|S_{11}|$. (b) AR.

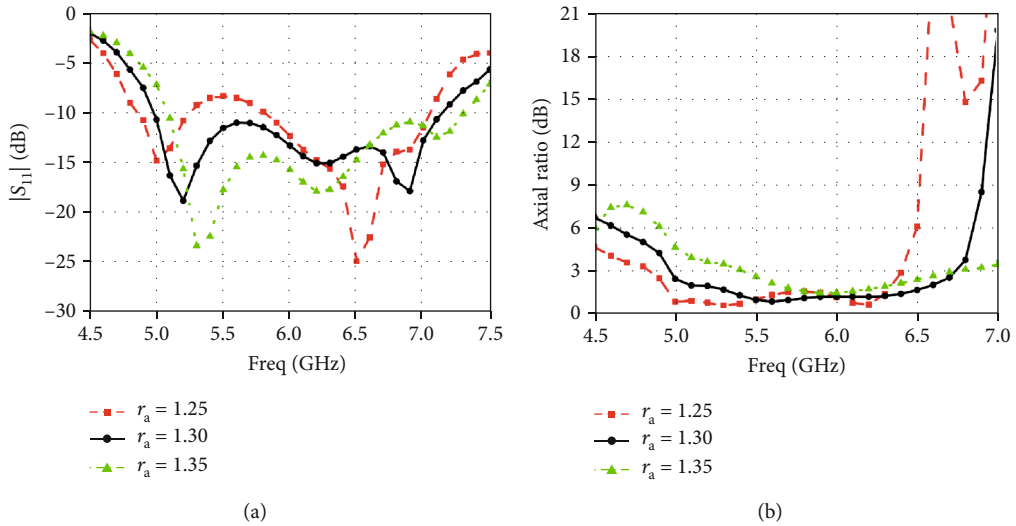

Figure 7: $|S_{11}|$ and AR with different values of r_a. (a) $|S_{11}|$. (b) AR.

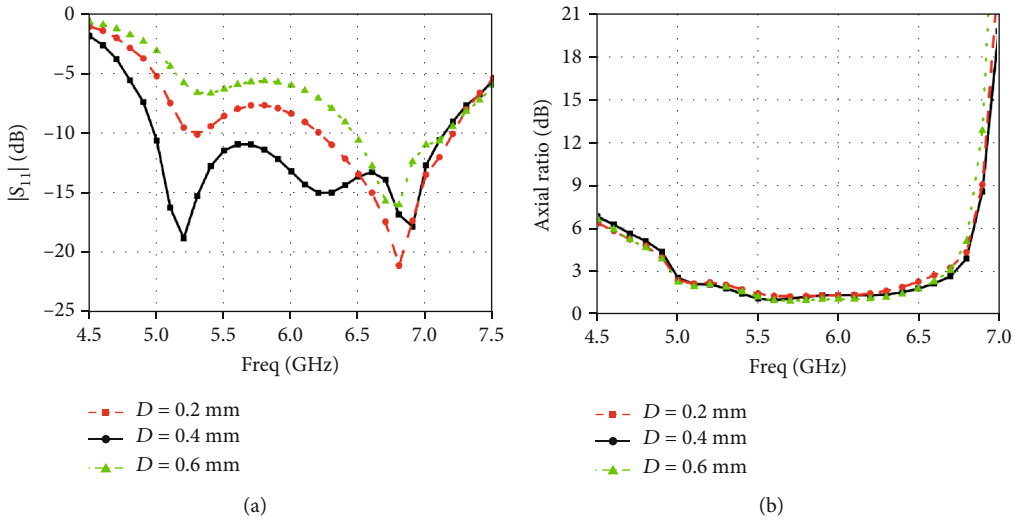

Figure 8: $|S_{11}|$ and AR with different values of D. (a) $|S_{11}|$. (b) AR.

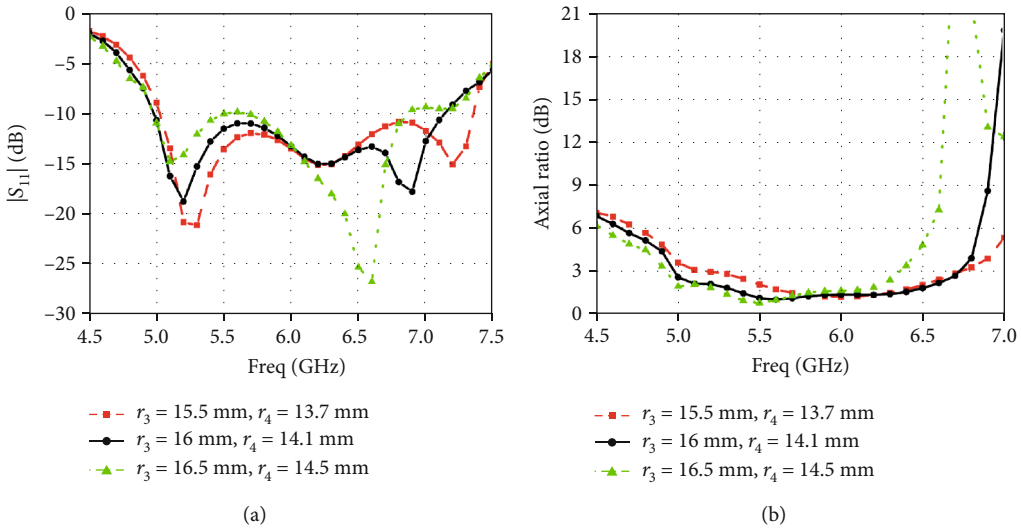

FIGURE 9: $|S_{11}|$ and AR with different values of r_5 and r_6. (a) $|S_{11}|$. (b) AR.

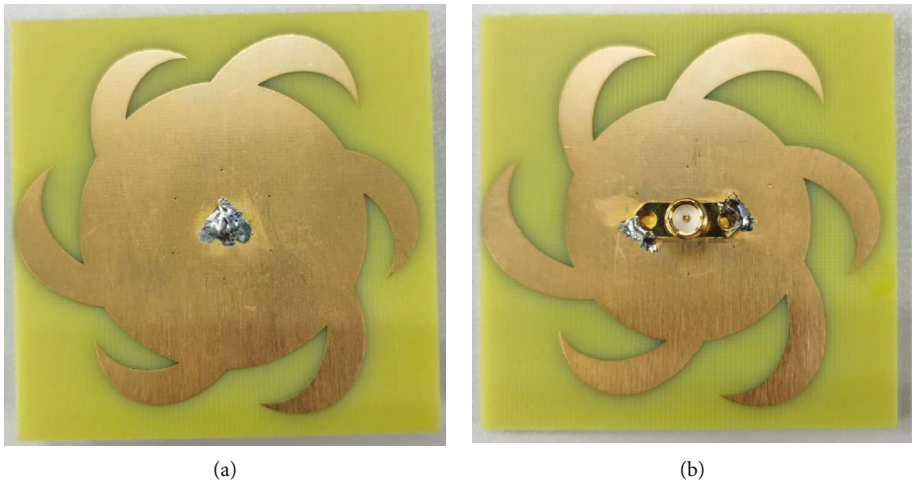

FIGURE 10: Prototype of the proposed antenna. (a) Top view. (b) Bottom view.

can produce a 90° phase difference between the horizontally polarized electric field and the vertically polarized electric field. Furthermore, the circular current can be excited on the arc-hook-shaped branches, as shown in Figure 2. The radiation pattern of the circular current is similar to that of a monopole current [23]. Therefore, the proposed antenna combined with the monopolar patch and arc-hook-shaped branches can generate conical-beam radiation in the elevation plane and omnidirectional radiation in some azimuth planes. The optimized geometrical parameters of the proposed antenna are given in Table 1.

To illustrate the advantages of the proposed approach, the design procedure of the proposed antenna is described. As shown in Figure 3, Ant. 1 is designed with a conventional monopolar patch antenna and a set of arc-hook-shaped branches connected to the ground plane. Each arc-hook-shaped branch in Ant. 1 has the same size. For Ant. 2, on the basis of Ant. 1, another set of arc-hook-shaped branches is connected to the upper patch, and this set of arc-hook-

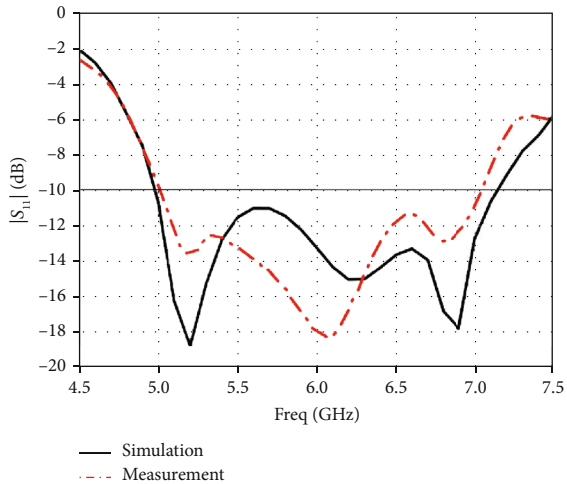

FIGURE 11: Simulated and measured $|S_{11}|$ for the fabricated antenna.

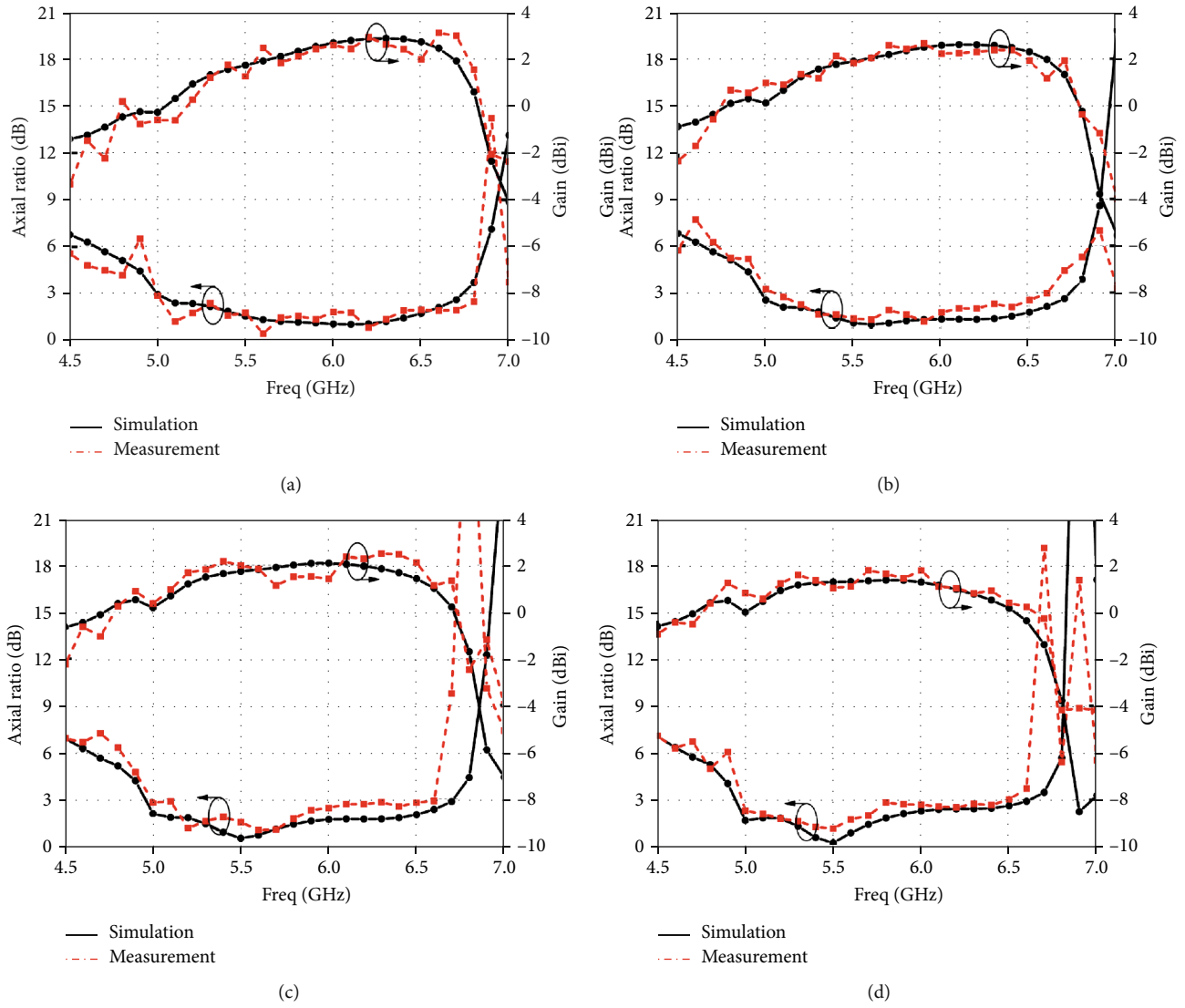

FIGURE 12: Simulated and measured AR and gain for the fabricated antenna at phi = 0° and different values of theta: (a) theta = 30°. (b) theta = 35°. (c) theta = 40°. (d) theta = 45°.

shaped branches is the mirror image relative to the y-axis (horizontal flip) of the set of arc-hook-shaped branches in Ant. 1. The size of each arc-hook-shaped branch in Ant. 2 is also the same. Ant. 3 is the proposed antenna, as mentioned before, which contains two types of arc-hook-shaped branches of different sizes. The three antennas are compared in terms of S_{11}, AR (at phi = 0° and theta = 35°), and radiation pattern performance which are shown in Figures 4(a), 4(b), and 5, respectively. From Figures 4(a) and 4(b), the impedance bandwidth (S_{11} < −10 dB) and AR bandwidth of Ant. 1 are 4.99-6.65 GHz (28.5%) and 4.63-6.97 GHz (40.3%), respectively. However, the AR bandwidth is not completely included in the impedance bandwidth below 4.99 GHz and above 6.65 GHz; thus the antenna cannot work in practice. For Ant. 2, although the AR bandwidth (5.47-6.67 GHz) is completely included in the impedance bandwidth (5.1-6.78 GHz), its overlap bandwidth is only 19.8%. For the proposed antenna (Ant. 3), when replacing the arc-hook-shaped branch of Ant. 2 with two types of arc-hook-shaped branches of different sizes, an additional resonance point can be generated compared to the Ant. 1 and Ant. 2. This allows Ant. 3 to achieve an AR bandwidth of 30.1% (4.97-6.73 GHz) and an impedance bandwidth of 35.6% (4.97-7.14 GHz). Even more prominent advantage of Ant. 3 is that the AR bandwidth is completely contained in the impedance bandwidth, and the overlap bandwidth is 30.1% (4.97-6.73 GHz). As shown in Figure 5, the three antennas can achieve a radiation pattern in the elevation plane of phi = 0° and omnidirectional radiation pattern in the azimuth plane of theta = 35°, respectively; however, compared with the Ant. 2 and Ant. 3, the radiation pattern of Ant. 1 is not symmetrical. According to the aforementioned analysis, the proposed antenna (Ant. 3) achieves the optimal overall performance.

To obtain the optimum electrical performance of the proposed antenna, parametric studies are introduced into the

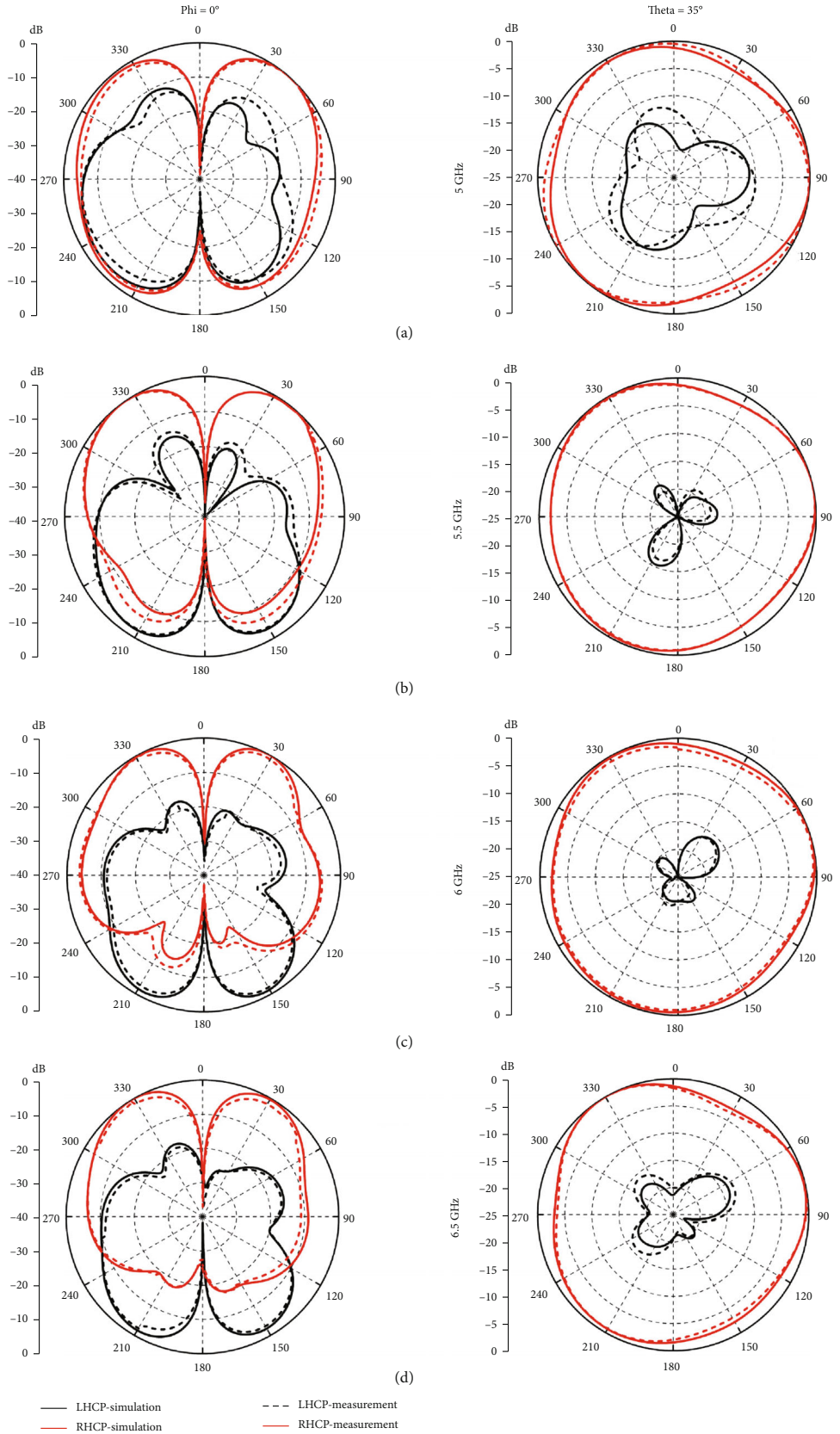

Figure 13: Simulated and measured radiation patterns for the fabricated antenna at different frequencies: (a) 5 GHz. (b) 5.5 GHz. (c) 6 GHz. (d) 6.5 GHz.

Table 2: Comparison of the proposed and other conical-beam CP antennas.

Ref.	Dimension of the antenna (λ^3)	Impedance bandwidth	AR bandwidth	Overlap bandwidth
[18]	$\Phi 1.47 \times 0.024$	19.8% (2.27-2.77 GHz)	19.3% (2.25-2.73 GHz)	18.4% (2.27-2.73 GHz)
[19]	$1.16 \times 1.16 \times 0.06$	28% (4.9-6.5 GHz)	14.4% (5.8-6.7 GHz)	11.4% (5.8-6.5 GHz)
[20]	$1.12 \times 1.12 \times 0.05$	19.6% (2.16-2.63 GHz)	27.4% (2.05-2.7 GHz)	19.6% (2.16-2.63 GHz)
[21]	$1.7 \times 1.7 \times 0.062$	21.9% (5.5-6.85 GHz)	15.9% (5.8-6.8 GHz)	15.9% (5.8-6.8 GHz)
[22]	$1.24 \times 1.24 \times 0.31$	17.5% (5.7-6.75 GHz)	26.5% (5.19-6.78 GHz)	17.5% (5.7-6.75 GHz)
This work	$1.08 \times 1.08 \times 0.05$	**35.6% (4.97-7.14 GHz)**	**30.1% (4.97-6.73 GHz)**	**30.1% (4.97-6.73 GHz)**

λ is the free space wavelength at the starting frequency of the overlap bandwidth.

design process. Considering the complexity of the antenna design, only several key parameters, such as the diameter of the shorting vias D, the ratio r_a, and the thickness of substrate H, are studied in this paper. Only one parameter is changed each time, while the others are fixed with the values shown in Table 1. Figure 6 illustrates the effects of the thickness of substrate H on the S_{11} and AR. The reason for this result is that the thickness of the substrate would affect not only the input impedance of the proposed antenna but also the amplitude of the two orthogonal electric fields. When $H = 3$ mm, the optimal results were obtained in terms of wide impedance and AR bandwidth. The effects of the ratio r_a on the S_{11} and AR are presented in Figure 7. As shown, when the ratio r_a is increased, the three resonance points (the frequency point with the lowest S_{11} value) move to the higher frequencies, the AR bandwidth also moves to the higher frequency band, and the AR values of lower frequency band will increase. When $r_a = 1.3$, the proposed antenna will obtain the optimal overlap bandwidth, i.e., the bandwidth of $|S_{11}| < -10$ dB and AR < 3 dB simultaneously. Figure 8 illustrates that the variation in the diameter of shorting via D has little effect on the AR bandwidth, but has a great effect on the impedance matching in the lower frequency band, and the optimal impedance bandwidth is obtained when $D = 0.2$ mm. In addition, in order to better illustrate the effect of different types of arc-hook-shaped branches on performances of the proposed antenna, the sizes of the two types of arc-hook-shaped branches are studied as shown in Figure 9. As can be seen, only the size of the Type-1 branch is changed here, while size of the Type-2 branch is kept constant. When the size of the Type-1 branch is increased, the impedance bandwidth is decreased, and when $r_3 = 16$ mm and $r_4 = 14.1$ mm, the proposed antenna can obtain the optimal AR bandwidth.

3. Simulation and Measurement Results

To prove the above design principles, a prototype has been fabricated by using PCB manufacturing process as shown in Figure 10. The S_{11} was measured using an Agilent N5071A vector network analyzer. The far-field performances such as AR, gain, and radiation pattern were measured in a microwave anechoic chamber.

Figure 11 shows the simulated and measured results of S_{11}. As shown, the measured impedance bandwidth of $|S_{11}| < -10$ dB is 33.6%, covering 5.01 to 7.03 GHz, while the simulated impedance bandwidth is 35.6% (4.97-7.14 GHz). There is a 2% deviation between the simulated and measured results, which may be caused by fabrication and measurement errors. The measured and simulated results of AR and gain at phi = 0° and theta = β ($\beta = 30°$, 35°, 40°, and 45°) are shown in Figure 12. From Figure 12, the measured results of AR and gain are in good agreement with the simulated results. And when the value of theta changes from 30° to 45°, the antenna still maintains a wide AR bandwidth. The AR bandwidths of proposed antenna at theta = 30°, 35°, 40°, and 45° are 29.6% (5-6.74 GHz), 30.1% (4.97-6.73 GHz), 29.9% (4.96-6.71 GHz), and 29.1% (4.94-6.62 GHz), respectively. The average gains within the operating bandwidth of the proposed antenna are 2.3 dBi, 2.0 dBi, 1.8 dBi, and 1.5 dBi, respectively. As can be seen in Figures 11 and 12, the overlap bandwidth of the proposed antenna at different values of theta can be maintained at about 30%, which is better than the antennas presented in the references mentioned above. The measured and simulated radiation patterns in the elevation (phi = 0°) and azimuth (theta = 35°) planes at 5, 5.5, 6, and 6.5 GHz are illustrated in Figure 13. As shown, the conical-beam radiation is achieved in the elevation plane while omnidirectional radiation is achieved in the azimuth plane at different frequencies.

To demonstrate the advantages of the proposed antenna, a comparison with other reported wideband CP conical-beam antennas is conducted and shown in Table 2. It can be seen that the proposed antenna has wider impedance, AR, and overlap ($|S_{11}| < -10$ dB and AR < 3 dB simultaneously) bandwidths than its counterparts.

4. Conclusions

A novel low-profile CP conical-beam antenna with wide overlap bandwidth has been proposed and analyzed. The proposed antenna is designed with a center fed wideband monopolar patch, six shorting vias, and two sets of arc-hook-shaped branches. Compared to the previous antennas, two types of arc-hook-shaped branches with different sizes are used, which can generate additional resonant frequency to enhance the overlap bandwidth (the bandwidth of $|S_{11}| < -10$ dB and AR < 3 dB simultaneously). The proposed antenna achieves an impedance bandwidth

($|S_{11}| < -10$ dB) of 35.6% (4.97-7.14 GHz) and a 3 dB axial ratio (AR) bandwidth at theta = 35° of about 30.1% (4.97-6.73 GHz). Moreover, the most important advantage of the proposed antenna is that the AR bandwidth is completely included in the impedance bandwidth, that is, the overlap bandwidth of $|S_{11}| < -10$ dB and AR < 3 dB is 30.1%. The conical-beam radiation is achieved in the elevation plane (phi = 0°), while the omnidirectional radiation is achieved in the azimuth plane (theta = 35°). Due to the wideband CP performance and conical-beam radiation feature, the proposed antenna is suitable for satellite, indoor, and vehicular communication systems.

Data Availability

The data used to support the findings of this study are included within the article.

Conflicts of Interest

The authors declare that there is no conflict of interest regarding the publication of this paper.

Acknowledgments

This work was supported in part by the National Natural Science Foundation of China under Grants 62071306, 61801299, and 61871433, in part by the Mobility Program for Taiwan Young Scientists under Grant RW2019TW001, and in part by the Shenzhen Science and Technology Program under Grants JCYJ20200109113601723, GJHZ20180418190529516, and JSGG20180507183215520.

References

[1] Y. He, W. He, and H. Wong, "A wideband circularly polarized cross-dipole antenna," *IEEE Antennas and Wireless Propagation Letters*, vol. 13, pp. 67–70, 2014.

[2] N. J. McEwan, R. A. Abd-Alhameed, E. M. Ibrahim, P. S. Excell, and J. G. Gardiner, "A new design of horizontally polarized and dual-polarized uniplanar conical beam antennas for HIPERLAN," *IEEE Transactions on Antennas and Propagation*, vol. 51, no. 2, pp. 229–237, 2003.

[3] B. Q. Wu and K.-M. Luk, "A wideband, low-profile, conical-beam antenna with horizontal polarization for indoor wireless communications," *IEEE Antennas and Wireless Propagation Letters*, vol. 8, pp. 634–636, 2009.

[4] J. Huang, "Circularly polarized conical patterns from circular microstrip antennas," *IEEE Transactions on Antennas and Propagation*, vol. 32, no. 9, pp. 991–994, 1984.

[5] H. Nakano, K. Vichien, T. Sugiura, and J. Yamauchi, "Singly-fed patch antenna radiating a circularly polarised conical beam," *Electronics Letters*, vol. 26, no. 10, pp. 638–640, 1990.

[6] W. Lin, H. Wong, and R. W. Ziolkowski, "Circularly polarized antenna with reconfigurable broadside and conical beams facilitated by a mode switchable feed network," *IEEE Transactions on Antennas and Propagation*, vol. 66, no. 2, pp. 996–1001, 2018.

[7] W. He, L. Zhang, Y. He et al., "An ultra-wideband circularly polarized asymmetric-*S* antenna with enhanced bandwidth and beamwidth performance," *IEEE Access*, vol. 7, pp. 134895–134902, 2019.

[8] S. S. Qi, W. Wu, and D. G. Fang, "Singly-fed circularly polarized circular aperture antenna with conical beam," *IEEE Transactions on Antennas and Propagation*, vol. 61, no. 6, pp. 3345–3349, 2013.

[9] C. Guo, R. Yang, and W. Zhang, "Compact omnidirectional circularly polarized antenna loaded with complementary V-shaped slits," *IEEE Antennas and Wireless Propagation Letters*, vol. 17, no. 9, pp. 1593–1597, 2018.

[10] D. Wu, X. Chen, L. Yang, G. Fu, and X. Shi, "Compact and low-profile omnidirectional circularly polarized antenna with four coupling arcs for UAV applications," *IEEE Antennas and Wireless Propagation Letters*, vol. 16, pp. 2919–2922, 2017.

[11] S. V. Kumar and A. R. Harish, "Generation of circularly polarized conical beam pattern using torus knot antenna," *IEEE Transactions on Antennas and Propagation*, vol. 65, no. 11, pp. 5740–5746, 2017.

[12] Y.-X. Guo and D. C. H. Tan, "Wideband single-feed circularly polarized patch antenna with conical radiation pattern," *IEEE Antennas and Wireless Propagation Letters*, vol. 8, pp. 924–926, 2009.

[13] X. Bai, X. Liang, M. Li, B. Zhou, J. Geng, and R. Jin, "Dual-circularly polarized conical-beam microstrip antenna," *IEEE Antennas and Wireless Propagation Letters*, vol. 14, pp. 482–485, 2015.

[14] Y. M. Pan and K. W. Leung, "Wideband circularly polarized dielectric bird-nest antenna with conical radiation pattern," *IEEE Transactions on Antennas and Propagation*, vol. 61, no. 2, pp. 563–570, 2013.

[15] S. Karki, M. Sabbadini, K. Alkhalifeh, and C. Craeye, "Metallic monopole parasitic antenna with circularly polarized conical patterns," *IEEE Transactions on Antennas and Propagation*, vol. 67, no. 8, pp. 5243–5252, 2019.

[16] T. Sharma, A. Rahman, S. Chakrabarti, and G. Barman, "Circularly polarized conical beam microstrip patch antenna at S-band," in *2015 IEEE Applied Electromagnetics Conference (AEMC)*, pp. 1-2, Guwahati, India, December 2015.

[17] H. H. Tran, N. Nguyen-Trong, and H. C. Park, "A compact wideband omnidirectional circularly polarized antenna using TM_{01} mode with capacitive feeding," *IEEE Antennas and Wireless Propagation Letters*, vol. 18, no. 1, pp. 19–23, 2019.

[18] Y. M. Pan, S. Y. Zheng, and B. J. Hu, "Wideband and low-profile omnidirectional circularly polarized patch antenna," *IEEE Transactions on Antennas and Propagation*, vol. 62, no. 8, pp. 4347–4351, 2014.

[19] W. Lin and H. Wong, "Circularly polarized conical-beam antenna with wide bandwidth and low profile," *IEEE Transactions on Antennas and Propagation*, vol. 62, no. 12, pp. 5974–5982, 2014.

[20] X. Chen, W. Zhang, L. Han, X. Chen, R. Ma, and G. Han, "Wideband circularly polarized antenna realizing omnidirectional radiation in the wider azimuth planes," *IEEE Antennas and Wireless Propagation Letters*, vol. 16, pp. 2461–2464, 2017.

[21] H. Xu, J. Zhou, Q. Wu, Z. Yu, and W. Hong, "Wideband low-profile SIW cavity-backed circularly polarized antenna with high-gain and conical beam radiation," *IEEE Transactions on Antennas and Propagation*, vol. 66, no. 3, pp. 1179–1188, 2018.

[22] W. He, L. Zhang, Y. He, and S. W. Wong, "A wideband circularly polarized antenna with conical-beam radiation," in *2019 IEEE International Conference on RFID Technology and Applications (RFID-TA)*, pp. 444–447, Pisa, Italy, September 2019.

[23] B. Li, S. Liao, and Q. Xue, "Omnidirectional circularly polarized antenna combining monopole and loop radiators," *IEEE Antennas and Wireless Propagation Letters*, vol. 12, pp. 607–610, 2013.